

Constant-time magic state distillation

Kwok Ho Wan

Universal Quantum, Gemini House, Mill Green Business Estate, Haywards Heath, UK, RH16 1XQ

We present numerical simulation results for the 7-to-1 and 15-to-1 state distillation circuits, constructed using transversal CNOTs acting on multiple surface code patches. The distillation circuits are decoded iteratively using the method outlined in [arXiv:2407.20976]. We show that, with a re-configurable qubit architecture, we can perform fast, $\mathcal{O}(1)$ code cycles magic state distillation. We confirm the error suppression ability of both distillation circuits, from input error rate $p \rightarrow \mathcal{O}(p^3)$ under circuit-level noise.

1 Introduction

The surface code [1–3] is a strong candidate for large scale fault-tolerant quantum computation. Every Clifford gate (H, S, CNOT) on the surface code permits a transversal implementation given a re-configurable hardware architecture or flying qubits [4], while the non-Clifford $T = \begin{pmatrix} 1 & 0 \\ 0 & e^{i\frac{\pi}{4}} \end{pmatrix}$ gate cannot be implemented transversally [5, 6]. One approach to bypass this restriction is to perform T gates via gate teleportation. This is achieved by consuming the magic state: $|T\rangle \propto |0\rangle + e^{i\frac{\pi}{4}}|1\rangle$ in the process.

Before the consumption of $|T\rangle$ state is possible, magic state injection techniques are needed to encode faulty logical $|T\rangle$ states from physical $|T\rangle$ states [7–10]. Then, the 15-to-1 distillation protocol (also known as distillation factory) is used to output a higher quality logical $|T\rangle$ state [11–13]. Similarly, another resource state: $|Y\rangle \propto |0\rangle + i|1\rangle$ can also be injected, distilled using the 7-to-1 distillation protocol [4, 14, 15] and consumed in a similar manner to perform the $S = \begin{pmatrix} 1 & 0 \\ 0 & i \end{pmatrix}$ gate. Lower overhead methods of initialising a high quality logical $|Y\rangle$ state has recently become available [16], this will potentially make the 7-

to-1 distillation protocol obsolete. Alternatively, the transversal logical S gate can be implemented with physical S, S^\dagger and CZ gates on the surface code [4, 17, 18]. Nevertheless, studying the 7-to-1 protocol can be insightful as the 7-to-1 and 15-to-1 protocols have many parallels.

In general, state distillation aims to use multiple faulty resource states with input error p , and output a higher quality $|T/Y\rangle$ state with suppressed output error rate of $p_{\text{out}} = \mathcal{O}(p^3)$. To leading order in p , $p \xrightarrow{15\text{-to-1}} 35p^3$ [11, 12] and $p \xrightarrow{7\text{-to-1}} 7p^3$ [14, 15]

Historically, state distillation protocols are the leading contributor to the spacetime volume footprint of a fault-tolerant quantum computer [3, 14, 15]. Magic state distillation using lattice surgery based technique requires a spacetime overhead of $\mathcal{O}(d^3)$ *qubit-cycles* (physical data qubits \times code cycles), where d is the distance of the surface code. This spacetime overhead had drastically decreased from $\mathcal{O}(1500d^3)$ [14, 15] to $\mathcal{O}(624d^3)$ [3] or $\mathcal{O}(396d^3)$ for the $|CCZ\rangle$ state distillation factory¹ [19]. However, all of the above mentioned state distillation schemes will output 1 $|T\rangle$ state (2 $|T\rangle$ states for the $|CCZ\rangle$ factory) every 5.5 d to 6.5 d code cycles. For larger code distances, the time complexity cost will pose run-time challenges to trapped-ions and neutral atoms qubit platforms, where the code cycle times are considerably slower, in the kHz regime [20–23] compared to MHz in superconducting platforms [24].

In order to bridge this three orders of magnitude gap in code cycle rate [4, 23, 25–29], we use the iterative transversal CNOT decoding technique from [30] to collapse the time complexity of both the 15-to-1 and 7-to-1 distillation protocols to $\mathcal{O}(1)$, removing its dependence on d . We numerically confirmed the 7-to-1 distillation simulation results from [4], without the need for a hyper-edge decoding graph or maximum like-

¹With a catalyst $|T\rangle$ state, the output state from a $|CCZ\rangle$ factory can be transformed into two $|T\rangle$ states.

likelihood decoders [4, 29]. In our approach, each surface code patch is decoded separately before iteratively propagating Pauli-frames from each corresponding patch [30]. Furthermore, we extended our approach to numerically characterise the 15-to-1 distillation protocol. Confirming the $p \rightarrow \mathcal{O}(p^3)$ scaling in both distillation protocols using stabiliser proxy.

We claim that the 7-to-1 and 15-to-1 distillation protocols can be implemented with $8d^2 \times 5 + 7d^2 = 47d^2$ and $16d^2 \times 6 + 15d^2 = 111d^2$ qubit-cycles respectively in re-configurable hardware platforms using the transversal CNOT decoder from [30]. These reported costs follow the convention from [31] and does not include both physical measurement ancilla qubits² and magic state injection cost. Our results provide a d times speed up for both distillation schemes compared to lattice surgery alternatives. In our simulations, we assume minimal shuttling and transversal CNOT errors. These assumptions will be further explored in works under preparation [32, 33].

This paper is structured as follows. Firstly, we introduce the 7-to-1 and 15-to-1 distillation circuits in section 2. Then, we present our contributions in section 3, simulating each distillation circuit with multiple surface code patches entangled with transversal CNOTs. Finally, we provide discussions and future directions in the last section.

2 State distillation protocols

In this section, we review the 7-to-1 and 15-to-1 distillation protocols and their underlying quantum error correcting codes: Steane and Reed-Muller code. We then discuss the post-selection protocol required in both distillation protocols to output an error suppressed distilled state.

The 15-to-1 $|T\rangle$ and 7-to-1 $|Y\rangle$ state distillation circuits are CNOT circuits followed by a resource state consumption stage, measurement and post-selection. They rely on the ability to perform specific gates via gate teleportation. This involves consuming many copies of faulty $|T\rangle$ ($|Y\rangle$) states and post-selecting measurement results to detect errors. One simple error is $Z \cdot T$ ($Z \cdot Y$) performed on the output state instead of T (Y).

Circuits from equation 1 show consumption of

²Double the qubit-cycles to include ancilla qubits [31].

$|-\rangle \propto |0\rangle - |1\rangle$, $|Y\rangle$ and $|T\rangle$ states to perform a Z , S and T gate respectively, up to measurement conditioned Clifford byproducts [34].

$$\begin{aligned}
 & \begin{array}{c} |\phi\rangle \\ |-\rangle \end{array} \begin{array}{c} \bullet \\ \oplus \end{array} \begin{array}{c} \text{---} \\ \text{---} \end{array} \begin{array}{c} (-1)^n Z |\phi\rangle \\ \text{---} \end{array} \\
 & \begin{array}{c} |\phi\rangle \\ |Y\rangle \end{array} \begin{array}{c} \bullet \\ \oplus \end{array} \begin{array}{c} \text{---} \\ \text{---} \end{array} \begin{array}{c} Z^n S |\phi\rangle \\ \text{---} \end{array} \\
 & \begin{array}{c} |\phi\rangle \\ |T\rangle \end{array} \begin{array}{c} \bullet \\ \oplus \end{array} \begin{array}{c} \text{---} \\ \text{---} \end{array} \begin{array}{c} (S^\dagger)^n T |\phi\rangle \\ \text{---} \end{array}
 \end{aligned} \tag{1}$$

The 7-to-1 $|Y\rangle$ and 15-to-1 $|T\rangle$ distillation protocols consume resource states needed to perform the S and T gates respectively. However, they also distill all resource states that perform integer powers of S and T respectively [13, 15]. The tuples, (resource state, gate by teleportation), below in equation 2 show what can be distilled by each protocol:

$$\begin{aligned}
 & \text{7-to-1 protocol: } \{(|-\rangle, Z), (|Y\rangle, S)\} \\
 & \text{15-to-1 protocol: } \{(|-\rangle, Z), (|Y\rangle, S), (|T\rangle, T)\}.
 \end{aligned} \tag{2}$$

In order to investigate the effectiveness of either distillation circuits, we looked at the stabiliser proxy of $|-\rangle$ state distillation using the 7-to-1 and 15-to-1 circuits in our numerical simulations. In practice, simple transversal implementation of the logical Z gate exists for surface code and will never realistically be performed in this manner with gate teleportation. We assume numerical results from $|-\rangle$ state distillation provide an order-of-magnitude estimation to the actual performance of $|Y\rangle$ or $|T\rangle$ state distillation. The true performance of any non-Clifford state distillation will have to be confirmed through experimental demonstrations on real hardware [10, 35].

We will now provide some background on the 7-to-1 and 15-to-1 distillation circuits along with the post-selection required to achieve the cubic error suppression. Unless otherwise specified, all the gates and measurements from this point onwards is understood to be in the surface code logical basis.

2.1 7-to-1 distillation protocol

The 7-to-1 distillation protocol relies on the $[[7, 1, 3]]$ Steane code's transversal S gate, \bar{S}_{Steane}

[36]. Figure 1 shows the Tanner graph of the self-dual Steane code. The encoding qubits are arranged as circular nodes, lying on the corners, mid-points and centroid of an equilateral triangle. The rectangular nodes are stabilisers (X or Z) of the code connected to qubits involved in each stabiliser check.

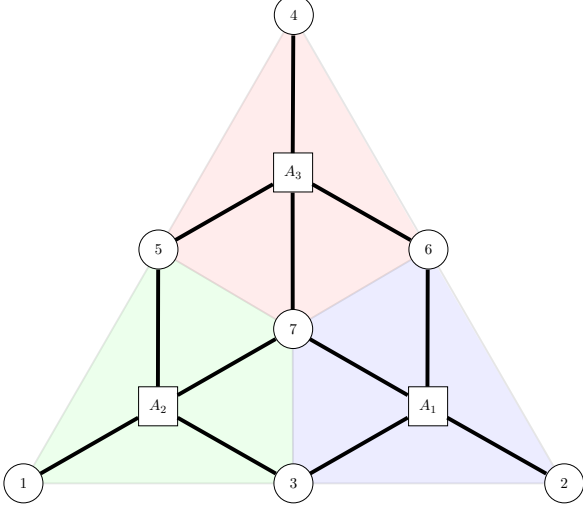


Figure 1: Tanner graph for the Steane code, encoded using 7 qubits arranged in the usual geometric manner on a triangle, rectangular nodes: $\{A_0, A_1, A_2\}$ are the self-dual X or Z stabiliser checks, while circular nodes 1-7 are the qubit labels.

We take the 7-to-1 distillation circuit (figure 2) from [4] with the first and fourth redundant transversal CNOTs removed. There is a one-to-one mapping of qubit labels between this circuit and qubit labels on the triangle in figure 1. The additional 0th qubit in the circuit is the output subsystem of this distillation circuit.

The 7-to-1 distillation circuit consists of 3 parallel layers of transversal CNOTs (separated by blue dotted lines in figure 2) performed on surface code patches initialised in the $|+\rangle$ or $|0\rangle$ state, followed by $|Y\rangle$ state consumption that perform S gates on patches 1 to 7, before measuring out the corresponding patches in the X or Z basis. Prior to the state consumption and readout stage, this circuit encodes the state stabilised by:

$$\left\langle X_0 \prod_{j=1}^7 X_j, Z_0 \prod_{j=1}^7 Z_j \right\rangle \cup \mathcal{G}_{\text{Steane}}, \quad (3)$$

$\overbrace{\prod_{j=1}^7 X_j}^{\bar{X}_{\text{Steane}}}$
 $\underbrace{\prod_{j=1}^7 Z_j}_{\bar{Z}_{\text{Steane}}}$

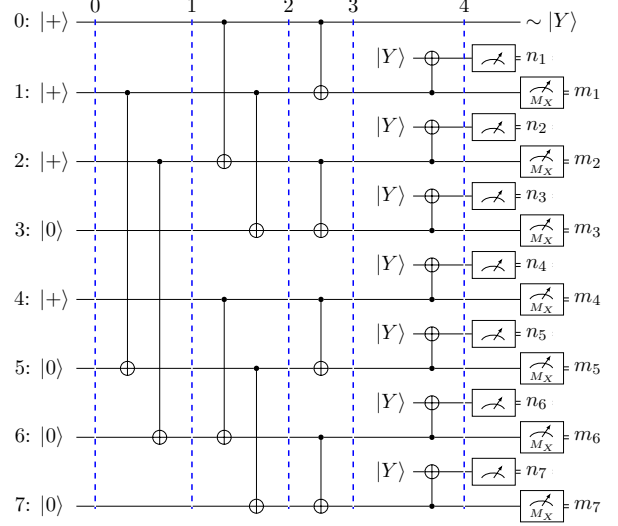


Figure 2: The 7-to-1 distillation circuit from [4] with the first and fourth redundant CNOTs removed as the CNOTs were acting on either $|+, +\rangle$ or $|0, 0\rangle$. A single round of syndrome extraction is inserted at every time step indicated by blue dotted lines in the surface code simulations.

$$\mathcal{G}_{\text{Steane}} = \left\langle X_1 X_3 X_5 X_7, X_2 X_3 X_6 X_7, \right. \\ \left. X_4 X_5 X_6 X_7, Z_1 Z_3 Z_5 Z_7, \right. \\ \left. Z_2 Z_3 Z_6 Z_7, Z_4 Z_5 Z_6 Z_7 \right\rangle, \quad (4)$$

where $\mathcal{G}_{\text{Steane}}$ consists of Steane code stabilisers and \bar{X}_{Steane} , \bar{Z}_{Steane} are the X , Z logical operators of the Steane code. Equation 3 is equivalent to a Bell state of the 0th surface code patch entangled with the Steane code encoded with patches 1 to 7. The state consumption stage uses 7 $|Y\rangle$ states to perform an S gate on surface code patches 1 to 7 through measurements in the Z basis (binary results n_j). This is equivalent to performing a \bar{S}_{Steane} gate at the Steane code level. After the Z measurements, the resulting state is stabilised by:

$$\left\langle (-Y_0) \bar{X}_{\text{Steane}} \cdot (-1)^{\sum_{k=1}^7 n_k}, \right. \\ \left. X_1 X_3 X_5 X_7 (-1)^{n_1+n_3+n_5+n_7}, \right. \\ \left. X_2 X_3 X_6 X_7 (-1)^{n_2+n_3+n_6+n_7}, \right. \\ \left. X_4 X_5 X_6 X_7 (-1)^{n_4+n_5+n_6+n_7} \right\rangle \\ \cup Z \text{ type operators.} \quad (5)$$

Next, perform the X basis measurements (binary results m_j), the output state is stabilised by:

$$\left\langle Y_0 \cdot (-1)^{\left(1+\sum_{k=1}^7 n_k+m_k\right)} \right\rangle. \quad (6)$$

Note that we have managed to force the 0th output surface code patch to be stabilised by Y_0 up to a \pm sign, depending on measurement results.

However, the input resource states or the distillation circuit can be faulty. The measurements results in the X and Z basis ($m_j, n_j \in \{0, 1\}$) are used to construct the Steane code stabilisers. These stabiliser measurement results will be used to post-select and identify erroneous output states.

See detailed discussion in [15] on the 7-to-1 post-selection procedure. In summary:

1. Construct the three weight-4 X type Steane code stabilisers:

$$\begin{aligned} X_1 X_3 X_5 X_7 &= \prod_{l \in \{n, m\}} (-1)^{l_1 + l_3 + l_5 + l_7} \\ X_2 X_3 X_6 X_7 &= \prod_{l \in \{n, m\}} (-1)^{l_2 + l_3 + l_6 + l_7} \\ X_4 X_5 X_6 X_7 &= \prod_{l \in \{n, m\}} (-1)^{l_4 + l_5 + l_6 + l_7}, \end{aligned} \quad (7)$$

with the measurement results (m_j, n_j) , post select on experiments when all 3 stabilisers returns the trivial results, i.e. $X_1 X_3 X_5 X_7 = X_2 X_3 X_6 X_7 = X_4 X_5 X_6 X_7 = 1$.

2. If $\prod_{j=1}^7 (-1)^{n_j + m_j} = 1$, there is an additional Z_0 Clifford offset to the 0th subsystem's Pauli-frame, which needs to be tracked (notice the sign of Y_0 in equation 6).

Successful post-selection outputs a $|Y\rangle$ state with suppressed error: $p_{\text{out}} = \mathcal{O}(7p^3)$, given $|Y\rangle$ resource states with input error rate p and a perfect distillation circuit. Assuming an error-free 7-to-1 distillation circuit, the full expression [4] for p_{out} is:

$$p_{\text{out}} = \frac{7p^3(1-p)^4 + p^7}{p^7 + (1-p)^7 + 7(1-p)^3p^4 + 7(1-p)^4p^3}. \quad (8)$$

Due to the post-selection procedure, a certain number of shots/experiments will be discarded. The number of shots discarded should be proportional to $\mathcal{O}(7p)$ at low error rates [4]. We will discuss simulation results concerning the 7-to-1 distillation circuit in section 3 and confirming its error suppression and discard ratio scaling under circuit-level noise.

2.2 15-to-1 distillation protocol

The 15-to-1 distillation protocol is enabled by the $[[15, 1, 3]]$ Reed-Muller code [37], which allows for a transversal T gate. This code has a geometric interpretation of qubits lying on the vertices of a tetrahedron complex, cellulated by four identical 6-sided polyhedron cells, in the configuration shown in figure 3. This code has four weight-8 X stabiliser checks specified by the cells of this tetrahedron, one example of a weight-8 X stabiliser check is shown in figure 4.

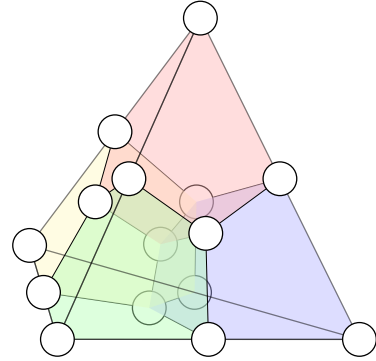


Figure 3: The $[[15, 1, 3]]$ Reed-Muller code's geometric representation with encoding qubits as circular nodes, rectangular stabiliser check nodes and its edges are excluded for representation purposes.

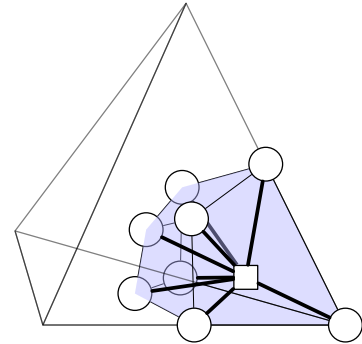


Figure 4: One of the four weight-8 X stabiliser check cells in the $[[15, 1, 3]]$ Reed-Muller code with the rectangular stabiliser check node explicitly shown.

The circuit in figure 5 is a construction of the 15-to-1 distillation protocol [38]. This circuit consists of 16 surface code patches initialised in the $|+\rangle$ or $|0\rangle$ state, before going through 4 parallel layers of CNOTs. This CNOT circuit (up until the blue dotted line labelled 4 in figure 5) generates a $r = 1$ Reed-Muller state, $|QMR_r\rangle$, from [38]. This 16 patch $|QMR_r\rangle$ state is a Bell state of the 0th surface code patch entangled with the

Reed-Muller code, stabilised by:

$$\langle X_0 \bar{X}_{\text{RM}}, Z_0 \bar{Z}_{\text{RM}} \rangle \cup \mathcal{G}_{\text{RM}}. \quad (9)$$

The generators \mathcal{G}_{RM} are the Reed-Muller code stabilisers and \bar{X}_{RM} and \bar{Z}_{RM} are the logical operator of the Reed-Muller code:

$$\bar{X}_{\text{RM}} = \prod_{j \in \text{Face}} X_j = \text{[Diagram of a tetrahedron with red dots on faces]}, \quad (10)$$

$$\bar{Z}_{\text{RM}} = \prod_{j \in \text{Edge}} Z_j = \text{[Diagram of a tetrahedron with blue dots on edges]}. \quad (11)$$

The operators \bar{X}_{RM} and \bar{Z}_{RM} are any weight-7 X -faces and any weight-3 Z -edge strings of the entire tetrahedron [37].

After the CNOT circuit, a logical T gate is performed at the Reed-Muller code level via consuming 15 surface code $|T\rangle$ states and measurements in the Z basis. Conditioned on the Z basis measurements, S gate(s) will be performed on the appropriate patch(es). This is followed by measurements in the X basis, in order to construct all four weight-8 X stabiliser checks of the Reed-Muller code:

$$\begin{aligned} &\langle X_1 X_3 X_5 X_7 X_9 X_{11} X_{13} X_{15}, \\ &X_2 X_3 X_6 X_7 X_{10} X_{11} X_{14} X_{15}, \\ &X_4 X_5 X_6 X_7 X_{12} X_{13} X_{14} X_{15}, \\ &X_8 X_9 X_{10} X_{11} X_{12} X_{13} X_{14} X_{15} \rangle. \end{aligned} \quad (12)$$

The measurement results are then post-selected upon the trivial result on all four stabiliser checks. The value of \bar{X}_{RM} , given by $M(\bar{X}_{\text{RM}})$ must also be constructed from these measurement results, as the final gate implemented on the 0th output patch is $T^{3-2M(\bar{X}_{\text{RM}})}$ [38].

Given 15 faulty $|T\rangle$ states with input error probability p , the error-free 15-to-1 distillation circuit suppresses the error of the output state to $\mathcal{O}(35p^3)$, with the full expression below [11]:

$$p_{\text{out}} = \frac{1 - 15(1 - 2p)^7 + 15(1 - 2p)^8 - (1 - 2p)^{15}}{2(1 + 15(1 - 2p)^8)}. \quad (13)$$

Similar to the 7-to-1 protocol, the post-selection procedure should discard $\mathcal{O}(15p)$ shots at low input error rates [38]. Both the error suppression and discard ratio scaling will be numerically

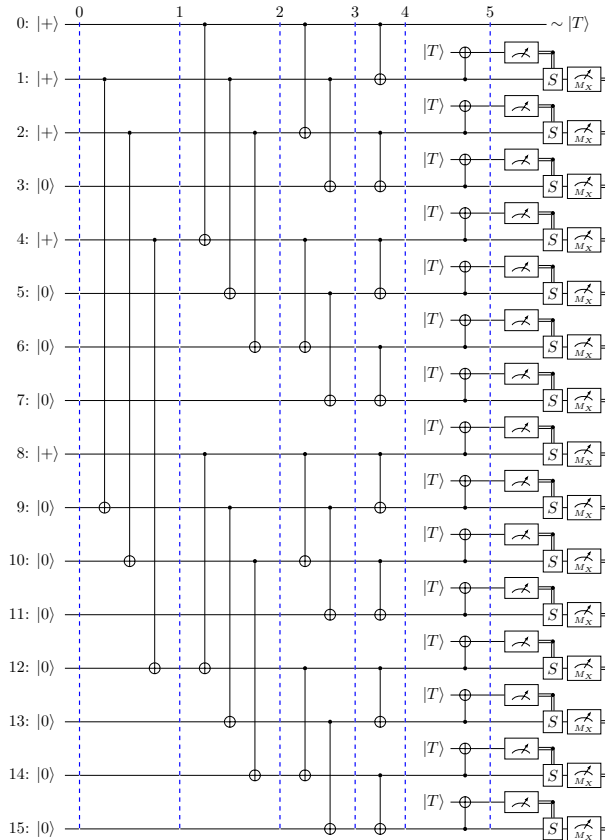


Figure 5: The 15-to-1 ($|T\rangle$ state) distillation circuit from [38] with all the redundant CNOTs removed. A single round of syndrome extraction is inserted at every time step indicated by blue dotted lines in the surface code simulations.

confirmed in section 3 later. Note that the 15-to-1 $|-\rangle$ state distillation does not require feed-forward S gates at the surface code level. This simplifies the numerical simulations, if a $|-\rangle$ state is consumed in place of a $|T\rangle$ state.

3 Surface code simulations

In this following section, we present our various numerical findings on the performance of both distillation circuits. One of the aims of this paper is to investigate whether the distillation error suppression scaling ($p \rightarrow \mathcal{O}(p^3)$) holds using surface code patches entangled with transversal CNOTs. We employ the iterative decoding scheme from [30] to decode the entire CNOT circuits in figure 2 and 5. In order to characterise the performance of each protocol, we distill the logical $|-\rangle$ state as a stabiliser proxy to the performance of either distillation circuits. In our simulations, we assume [30]:

1. Error-free and instantaneous transversal CNOTs (transversal CNOT errors can be subsumed into a marginally larger circuit-level noise).
2. Standard SD6 circuit-level depolarising noise model [39, 40] on all gates except the resource state initialisation errors.
3. Artificial injection of Z input errors [4] (with probability p) on all resource states to be consumed.

Interestingly, one can perform an inplace Y basis measurement on the surface code [10, 16, 41], this can also be used to benchmark both distillation protocols [32, 33].

We demonstrate that the iterative decoding scheme from [30] can perform well in the context of state distillation. Furthermore, we propose a time complexity speed up given a re-configurable qubit platform such as trapped-ions [27, 28] with the ability to perform long-range two qubit gates.

We use Stim [42] to construct and sample the logical circuits from figures 2 and 5, we decoded each surface code patch separately using PyMatching [43] and propagate the Pauli-frames accordingly when a transversal logical CNOT is applied. No more than 3 global iterations of the algorithm provided in [30] was needed in all of the following simulations. A single round of syndrome extraction is inserted on all the logical qubits at every time step labelled with blue dotted lines in figures 2 and 5. We benchmark the circuits by computing the stabiliser proxy of distilling a logical $|-\rangle$ state. We treat this as an order-of-magnitude estimation for the true performance of state distillation when logical $|Y\rangle$ or $|T\rangle$ states are involved.

The output error rates for the 7-to-1 circuit (figure 6) and the 15-to-1 circuit (figure 7) matches the expected $\mathcal{O}(p^3)$ scaling well. We simulated the 7-to-1 circuit from [4], however we noticed that the first and fourth CNOTs applied in [4] are redundant as they act on either $|0, 0\rangle$ or $|+, +\rangle$, hence these gates are removed in our simulations. We confirmed the single level distillation factory results from [4] at circuit-level noise $p_{\text{circuit}} = 0.1\%$. We noticed similar deviation from the zero circuit-level noise curve over a range of distances $d \in \{3, 5, 7, 9\}$. Furthermore, we also notice similar deviations in our 15-to-1 circuit simulations. This is due to circuit-

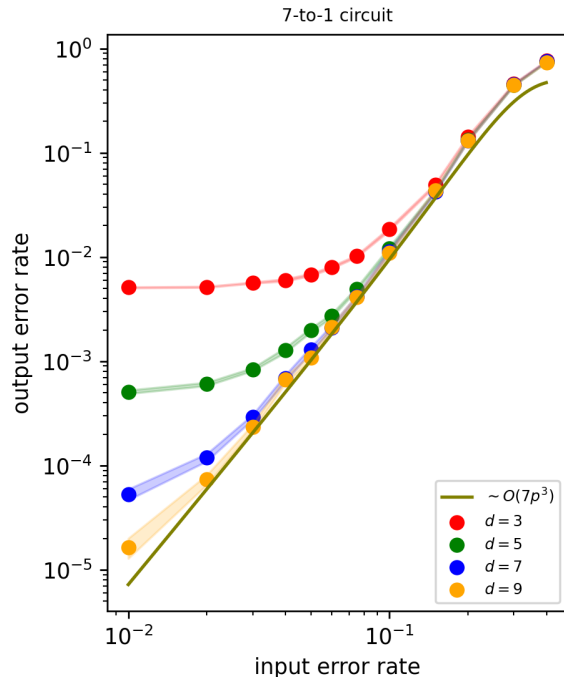


Figure 6: Surface code simulations of the 7-to-1 distillation output error rate. The output error scaling: $\mathcal{O}(7p^3)$ is confirmed across distances $d \in \{3, 5, 7, 9\}$ at 0.1% circuit-level noise.

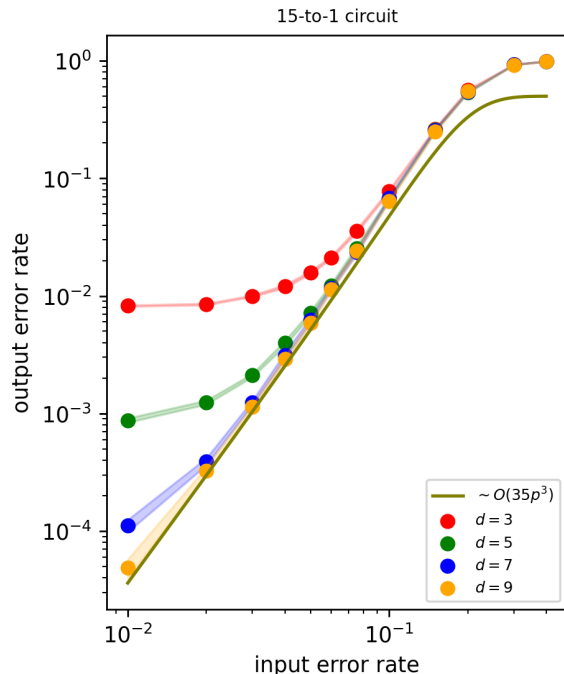


Figure 7: Surface code simulations of the 15-to-1 distillation output error rate. The output error scaling: $\mathcal{O}(35p^3)$ is confirmed across distances $d \in \{3, 5, 7, 9\}$ at 0.1% circuit-level noise.

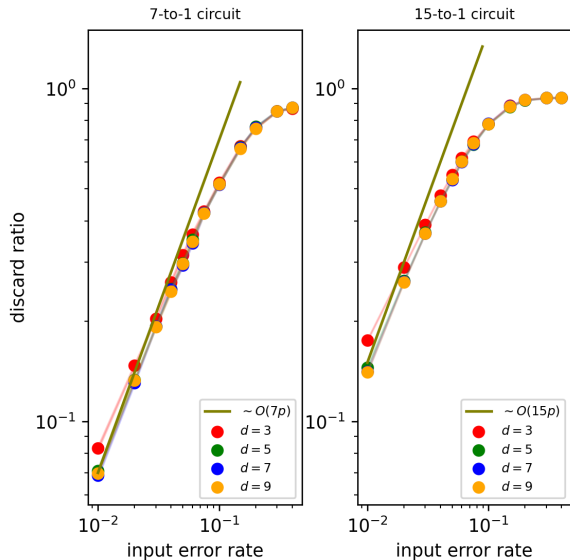


Figure 8: The discard ratio of the 7-to-1 circuit (left) and 15-to-1 circuit (right) stemming from the surface code simulations. We confirm the discard ratio of $\mathcal{O}(7p)$ and $\mathcal{O}(15p)$ at low input error rate p for both distillation protocols.

level noise imperfections similar to the findings from [4]. For different surface code distances, the output error rate seems to plateau at specific values. Further work is needed to extract the behaviour between distance vs plateau value with more computational power at lower input error rates and higher distances. Additionally, we also confirm the discard ratios at the post-selection stage of both distillation protocols at low input error rates, as shown in figure 8. In addition to the previous numerical simulations, we also computed the overall logical fidelity of the pure CNOT sub-circuit component of either distillation protocols. The logical error rate in figure 9 is defined to be the transversal CNOT sub-circuit logical failure rate benchmarked using stabiliser-flow/Pauli-web [30, 44, 45]. Close agreement of logical error rates compared to the equivalent idling memory experiment is observed in both distillation CNOT sub-circuits (figure 9).

All the above numerical evidences suggest that the distillation circuits can suppress errors with the correct scaling in the presence of circuit-level noise when decoded using [30]. In re-configurable hardware platforms with minimal shuttling fidelity degradation, the 15-to-1 distillation protocol³ can be performed with 6 code cycles, 15 logi-

³Without the conditional transversal S gates [4, 17, 18].

cal qubits and 15 $|T\rangle$ states to be consumed. This implies a total qubit-cycle of $16d^2 \times 6 + 15d^2 = 111d^2$ excluding physical ancilla qubits and magic state injection cost. Likewise, the 7-to-1 distillation protocol spacetime cost is: $8d^2 \times 5 + 7d^2 = 47d^2$ qubit-cycles with similar constructions.

4 Discussions and outlook

The numerical simulation results in this manuscript address the feasibility of using long-range transversal CNOT operations to perform magic state distillation with the surface code.

The crux of this study is to confirm the error suppression scaling: $p \xrightarrow{15\text{-to-1}} 35p^3$ and $p \xrightarrow{7\text{-to-1}} 7p^3$, under circuit-level noise with injected Z input logical error of strength p . Our results show that a single-level distillation factory can indeed suppress error, and distill resource states when paired with the decoder from [30]. We remark that each surface code patch is decoded separately, with appropriate propagation of Pauli-frames. No more than 3 global rounds of iterative decoding is needed in either distillation circuit simulations. Our numerical results suggest that fast $\mathcal{O}(1)$ code cycles magic state distillation can be made possible on re-configurable qubit platforms. However, the true magic state distillation performance will have to be confirmed in experiments [10, 41] as no efficient large scale non-Clifford simulation algorithm exists [46].

This work provides a step towards realistic implementation of time-optimal magic state distillation on re-configurable hardware architectures. Future works on implementing an inplace Y basis measurement will allow for more accurate performance benchmark of both factories. In addition, analysis of hardware realistic connectivity error models is under preparation [32, 33].

Recent work on magic state cultivation [10] promises high quality injected (‘cultivated’) magic state at logical error rate as low as 2×10^{-9} with 0.1% circuit-level noise. This can potentially make multi-level magic state distillation obsolete. However, many fault-tolerant quantum algorithms require T-count greater than $\frac{1}{2 \times 10^{-9}} = 5 \times 10^8$ [47]. Single-level magic state distillation might still be vital in suppressing error rates from $2 \times 10^{-9} \xrightarrow{15\text{-to-1}} 2.8 \times 10^{-25}$. Incorporating an end-to-end analysis of magic state cultivation followed by transversal CNOT enabled magic state

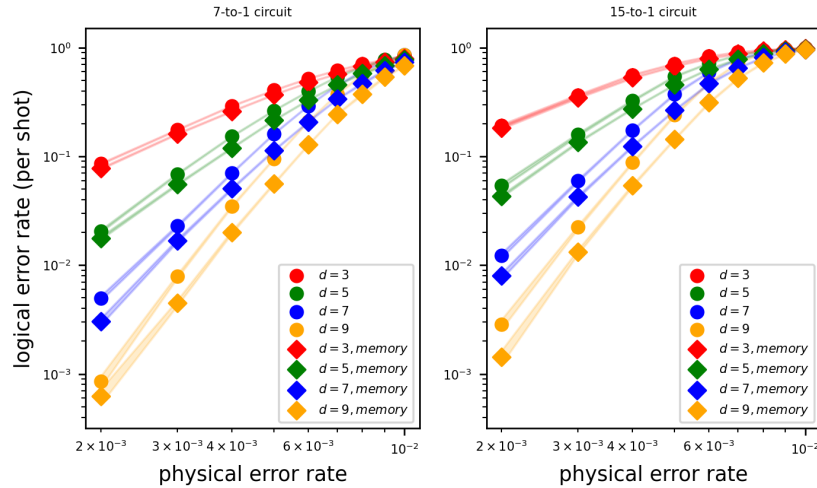


Figure 9: Logical error rate comparisons of the 7-to-1 (left) and 15-to-1 (right) pure CNOT sub-circuits against an equivalent memory experiment with the same number of syndrome extraction rounds.

distillation is a fruitful topic to study.

5 Acknowledgments

We acknowledge discussions with Mark Webber. We also want to thank all our colleagues at Universal Quantum Ltd for creating an environment where this research was made possible. The numerical simulations were performed on a 2023 version Dell XPS17 laptop with an Intel Core i7-12700H (14 cores) processor and 64 GB of physical memory (RAM). The tikzpicture code used to construct the tetrahedron is a modified version of the code available at [48].

References

- [1] Eric Dennis, Alexei Kitaev, Andrew Landahl, and John Preskill. Topological quantum memory. *Journal of Mathematical Physics*, 43(9):4452–4505, September 2002. ISSN 1089-7658. DOI: [10.1063/1.1499754](https://doi.org/10.1063/1.1499754). URL <http://dx.doi.org/10.1063/1.1499754>.
- [2] Austin G. Fowler, Matteo Mariantoni, John M. Martinis, and Andrew N. Cleland. Surface codes: Towards practical large-scale quantum computation. *Physical Review A*, 86(3), September 2012. ISSN 1094-1622. DOI: [10.1103/PhysRevA.86.032324](https://doi.org/10.1103/PhysRevA.86.032324). URL <http://dx.doi.org/10.1103/PhysRevA.86.032324>.
- [3] Austin G. Fowler and Craig Gidney. Low overhead quantum computation using lattice surgery, 2019. URL <https://arxiv.org/abs/1808.06709>.
- [4] Hengyun Zhou, Chen Zhao, Madelyn Cain, Dolev Bluvstein, Casey Duckering, Hong-Ye Hu, Sheng-Tao Wang, Aleksander Kubica, and Mikhail D. Lukin. Algorithmic fault tolerance for fast quantum computing, 2024. URL <https://arxiv.org/abs/2406.17653>.
- [5] Bryan Eastin and Emanuel Knill. Restrictions on transversal encoded quantum gate sets. *Phys. Rev. Lett.*, 102:110502, Mar 2009. DOI: [10.1103/PhysRevLett.102.110502](https://doi.org/10.1103/PhysRevLett.102.110502). URL <https://link.aps.org/doi/10.1103/PhysRevLett.102.110502>.
- [6] Sergey Bravyi and Robert König. Classification of topologically protected gates for local stabilizer codes. *Phys. Rev. Lett.*, 110:170503, Apr 2013. DOI: [10.1103/PhysRevLett.110.170503](https://doi.org/10.1103/PhysRevLett.110.170503). URL <https://link.aps.org/doi/10.1103/PhysRevLett.110.170503>.
- [7] Ying Li. A magic state’s fidelity can be superior to the operations that created it. *New Journal of Physics*, 17(2):023037, February 2015. ISSN 1367-2630. DOI: [10.1088/1367-2630/17/2/023037](https://doi.org/10.1088/1367-2630/17/2/023037). URL <http://dx.doi.org/10.1088/1367-2630/17/2/023037>.
- [8] Lingling Lao and Ben Criger. Magic state injection on the rotated surface code. In *Proceedings of the 19th ACM Inter-*

- national Conference on Computing Frontiers*, CF '22, page 113–120, New York, NY, USA, 2022. Association for Computing Machinery. ISBN 9781450393386. DOI: [10.1145/3528416.3530237](https://doi.org/10.1145/3528416.3530237). URL <https://doi.org/10.1145/3528416.3530237>.
- [9] Héctor Bombín, Mihir Pant, Sam Roberts, and Karthik I. Seetharam. Fault-tolerant postselection for low-overhead magic state preparation. *PRX Quantum*, 5:010302, Jan 2024. DOI: [10.1103/PRXQuantum.5.010302](https://doi.org/10.1103/PRXQuantum.5.010302). URL <https://link.aps.org/doi/10.1103/PRXQuantum.5.010302>.
- [10] Craig Gidney, Noah ShuTTY, and Cody Jones. Magic state cultivation: growing T states as cheap as CNOT gates, 2024. URL <https://arxiv.org/abs/2409.17595>.
- [11] Sergey Bravyi and Alexei Kitaev. Universal quantum computation with ideal clifford gates and noisy ancillas. *Phys. Rev. A*, 71:022316, Feb 2005. DOI: [10.1103/PhysRevA.71.022316](https://doi.org/10.1103/PhysRevA.71.022316). URL <https://link.aps.org/doi/10.1103/PhysRevA.71.022316>.
- [12] Sergey Bravyi and Jeongwan Haah. Magic-state distillation with low overhead. *Physical Review A*, 86(5), November 2012. ISSN 1094-1622. DOI: [10.1103/PhysRevA.86.052329](https://doi.org/10.1103/PhysRevA.86.052329). URL <http://dx.doi.org/10.1103/PhysRevA.86.052329>.
- [13] Jeongwan Haah and Matthew B. Hastings. Codes and Protocols for Distilling T , controlled- S , and Toffoli Gates. *Quantum*, 2:71, June 2018. ISSN 2521-327X. DOI: [10.22331/q-2018-06-07-71](https://doi.org/10.22331/q-2018-06-07-71). URL <https://doi.org/10.22331/q-2018-06-07-71>.
- [14] Austin G. Fowler and Simon J. Devitt. A bridge to lower overhead quantum computation, 2013. URL <https://arxiv.org/abs/1209.0510>.
- [15] Daniel Herr, Franco Nori, and Simon J Devitt. Lattice surgery translation for quantum computation. *New Journal of Physics*, 19(1):013034, January 2017. ISSN 1367-2630. DOI: [10.1088/1367-2630/aa5709](https://doi.org/10.1088/1367-2630/aa5709). URL <http://dx.doi.org/10.1088/1367-2630/aa5709>.
- [16] Craig Gidney. Inplace access to the surface code Y basis. *Quantum*, 8:1310, April 2024. ISSN 2521-327X. DOI: [10.22331/q-2024-04-08-1310](https://doi.org/10.22331/q-2024-04-08-1310). URL <http://dx.doi.org/10.22331/q-2024-04-08-1310>.
- [17] Jonathan E. Moussa. Transversal clifford gates on folded surface codes. *Phys. Rev. A*, 94:042316, Oct 2016. DOI: [10.1103/PhysRevA.94.042316](https://doi.org/10.1103/PhysRevA.94.042316). URL <https://link.aps.org/doi/10.1103/PhysRevA.94.042316>.
- [18] Nikolas P. Breuckmann and Simon Burton. Fold-transversal clifford gates for quantum codes. *Quantum*, 8:1372, June 2024. ISSN 2521-327X. DOI: [10.22331/q-2024-06-13-1372](https://doi.org/10.22331/q-2024-06-13-1372). URL <http://dx.doi.org/10.22331/q-2024-06-13-1372>.
- [19] Craig Gidney and Austin G. Fowler. Efficient magic state factories with a catalyzed $|CCZ\rangle$ to $2|T\rangle$ transformation. *Quantum*, 3:135, April 2019. ISSN 2521-327X. DOI: [10.22331/q-2019-04-30-135](https://doi.org/10.22331/q-2019-04-30-135). URL <https://doi.org/10.22331/q-2019-04-30-135>.
- [20] Lukas Postler, Friederike Butt, Ivan Pogorelov, Christian D. Marciniak, Sascha Heußen, Rainer Blatt, Philipp Schindler, Manuel Rispler, Markus Müller, and Thomas Monz. Demonstration of fault-tolerant steane quantum error correction, 2023. URL <https://arxiv.org/abs/2312.09745>.
- [21] C. Ryan-Anderson, J. G. Bohnet, K. Lee, D. Gresh, A. Hankin, J. P. Gaebler, D. Francois, A. Chernoguzov, D. Lucchetti, N. C. Brown, T. M. Gatterman, S. K. Halit, K. Gilmore, J. A. Gerber, B. Neyenhuis, D. Hayes, and R. P. Stutz. Realization of real-time fault-tolerant quantum error correction. *Phys. Rev. X*, 11:041058, Dec 2021. DOI: [10.1103/PhysRevX.11.041058](https://doi.org/10.1103/PhysRevX.11.041058). URL <https://link.aps.org/doi/10.1103/PhysRevX.11.041058>.
- [22] C. Ryan-Anderson, N. C. Brown, C. H. Baldwin, J. M. Dreiling, C. Foltz, J. P. Gaebler, T. M. Gatterman, N. Hewitt, C. Holliman, C. V. Horst, J. Johansen, D. Lucchetti, T. Mengle, M. Matheny, Y. Matsuoka, K. Mayer, M. Mills, S. A. Moses, B. Neyenhuis, J. Pino, P. Siegfried, R. P. Stutz, J. Walker, and D. Hayes. High-fidelity and fault-tolerant teleportation of a logical qubit using transversal gates and lattice surgery on a trapped-ion quantum computer, 2024. URL <https://arxiv.org/abs/2404.16728>.
- [23] Dolev Bluvstein, Simon J. Evered, Alexandra A. Geim, Sophie H. Li, Hengyun

Zhou, Tom Manovitz, Sepehr Ebadi, Madelyn Cain, Marcin Kalinowski, Dominik Hangleiter, J. Pablo Bonilla Ataides, Nishad Maskara, Iris Cong, Xun Gao, Pedro Sales Rodriguez, Thomas Karolyshyn, Giulia Semeghini, Michael J. Gullans, Markus Greiner, Vladan Vuletić, and Mikhail D. Lukin. Logical quantum processor based on reconfigurable atom arrays. *Nature*, 626(7997):58–65, Feb 2024. ISSN 1476-4687. DOI: [10.1038/s41586-023-06927-3](https://doi.org/10.1038/s41586-023-06927-3). URL <https://doi.org/10.1038/s41586-023-06927-3>.

[24] Rajeev Acharya, Laleh Aghababaie-Beni, Igor Aleiner, Trond I. Andersen, Markus Ansmann, Frank Arute, Kunal Arya, Abraham Asfaw, Nikita Astrakhantsev, Juan Atalaya, Ryan Babbush, Dave Bacon, Brian Ballard, Joseph C. Bardin, Johannes Bausch, Andreas Bengtsson, Alexander Bilmes, Sam Blackwell, Sergio Boixo, Gina Bortoli, Alexandre Bourassa, Jenna Bovaird, Leon Brill, Michael Broughton, David A. Browne, Brett Buchea, Bob B. Buckley, David A. Buell, Tim Burger, Brian Burkett, Nicholas Bushnell, Anthony Cabrera, Juan Campero, Hung-Shen Chang, Yu Chen, Zijun Chen, Ben Chiaro, Desmond Chik, Charina Chou, Jahan Claes, Agnetta Y. Cleland, Josh Cogan, Roberto Collins, Paul Conner, William Courtney, Alexander L. Crook, Ben Curtin, Sayan Das, Alex Davies, Laura De Lorenzo, Dripto M. Debroy, Sean Demura, Michel Devoret, Agustin Di Paolo, Paul Donohoe, Ilya Drozdov, Andrew Dunsworth, Clint Earle, Thomas Edlich, Alec Eickbusch, Aviv Moshe Elbag, Mahmoud Elzouka, Catherine Erickson, Lara Faoro, Edward Farhi, Vinicius S. Ferreira, Leslie Flores Burgos, Ebrahim Forati, Austin G. Fowler, Brooks Foxen, Suhas Ganjam, Gonzalo Garcia, Robert Gasca, Élie Genois, William Giang, Craig Gidney, Dar Gilboa, Raja Gosula, Alejandro Grajales Dau, Dietrich Graumann, Alex Greene, Jonathan A. Gross, Steve Habegger, John Hall, Michael C. Hamilton, Monica Hansen, Matthew P. Harrigan, Sean D. Harrington, Francisco J. H. Heras, Stephen Heslin, Paula Heu, Oscar Higgott, Gordon Hill, Jeremy Hilton, George Holland,

Sabrina Hong, Hsin-Yuan Huang, Ashley Huff, William J. Huggins, Lev B. Ioffe, Sergei V. Isakov, Justin Iveland, Evan Jeffrey, Zhang Jiang, Cody Jones, Stephen Jordan, Chaitali Joshi, Pavol Juhas, Dvir Kafri, Hui Kang, Amir H. Karamlou, Kostyantyn Kechedzhi, Julian Kelly, Trupti Khairé, Tanuj Khattar, Mostafa Khezri, Seon Kim, Paul V. Klimov, Andrey R. Klots, Bryce Kobrin, Pushmeet Kohli, Alexander N. Korotkov, Fedor Kostritsa, Robin Kothari, Borislav Kozlovskii, John Mark Kreikebaum, Vladislav D. Kurilovich, Nathan Lacroix, David Landhuis, Tiano Lange-Dei, Brandon W. Langley, Pavel Laptev, Kim-Ming Lau, Loïck Le Guevel, Justin Ledford, Kenny Lee, Yuri D. Lensky, Shannon Leon, Brian J. Lester, Wing Yan Li, Yin Li, Alexander T. Lill, Wayne Liu, William P. Livingston, Aditya Locharla, Erik Lucero, Daniel Lundahl, Aaron Lunt, Sid Madhuk, Fionn D. Malone, Ashley Maloney, Salvatore Mandrà, Leigh S. Martin, Steven Martin, Orion Martin, Cameron Maxfield, Jarrod R. McClean, Matt McEwen, Seneca Meeks, Anthony Megrant, Xiao Mi, Kevin C. Miao, Amanda Mieszala, Reza Molavi, Sebastian Molina, Shirin Montazeri, Alexis Morvan, Ramis Movasagh, Wojciech Mruzekiewicz, Ofer Naaman, Matthew Neeley, Charles Neill, Ani Nersisyan, Hartmut Neven, Michael Newman, Jiun How Ng, Anthony Nguyen, Murray Nguyen, Chia-Hung Ni, Thomas E. O’Brien, William D. Oliver, Alex Opremcak, Kristoffer Ottosson, Andre Petukhov, Alex Pizzuto, John Platt, Rebecca Potter, Orion Pritchard, Leonid P. Pryadko, Chris Quintana, Ganesh Ramachandran, Matthew J. Reagor, David M. Rhodes, Gabrielle Roberts, Elliott Rosenberg, Emma Rosenfeld, Pedram Roushan, Nicholas C. Rubin, Negar Saei, Daniel Sank, Kannan Sankaragomathi, Kevin J. Satzinger, Henry F. Schurkus, Christopher Schuster, Andrew W. Senior, Michael J. Shearn, Aaron Shorter, Noah Shuttly, Vladimir Shvarts, Shraddha Singh, Volodymyr Sivak, Jindra Skruzny, Spencer Small, Vadim Smelyanskiy, W. Clarke Smith, Rolando D. Somma, Sofia Springer, George Sterling,

- Doug Strain, Jordan Suchard, Aaron Szasz, Alex Sztein, Douglas Thor, Alfredo Torres, M. Mert Torunbalci, Abeer Vaishnav, Justin Vargas, Sergey Vdovichev, Guifre Vidal, Benjamin Villalonga, Catherine Vollgraff Heidweiller, Steven Waltman, Shannon X. Wang, Brayden Ware, Kate Weber, Theodore White, Kristi Wong, Bryan W. K. Woo, Cheng Xing, Z. Jamie Yao, Ping Yeh, Bicheng Ying, Juhwan Yoo, Noureldin Yosri, Grayson Young, Adam Zalcman, Yaxing Zhang, Ningfeng Zhu, and Nicholas Zobrist. Quantum error correction below the surface code threshold, 2024. URL <https://arxiv.org/abs/2408.13687>.
- [25] Mark Webber, Vincent Elfving, Sebastian Weidt, and Winfried K. Hensinger. The impact of hardware specifications on reaching quantum advantage in the fault tolerant regime. *AVS Quantum Science*, 4(1), January 2022. ISSN 2639-0213. DOI: [10.1116/5.0073075](https://doi.org/10.1116/5.0073075). URL <http://dx.doi.org/10.1116/5.0073075>.
- [26] Mark Webber, Steven Herbert, Sebastian Weidt, and Winfried K. Hensinger. Efficient qubit routing for a globally connected trapped ion quantum computer. *Advanced Quantum Technologies*, 3(8):2000027, 2020. DOI: <https://doi.org/10.1002/qute.202000027>. URL <https://onlinelibrary.wiley.com/doi/abs/10.1002/qute.202000027>.
- [27] Bjoern Lekitsch, Sebastian Weidt, Austin G. Fowler, Klaus Mølmer, Simon J. Devitt, Christof Wunderlich, and Winfried K. Hensinger. Blueprint for a microwave trapped ion quantum computer. *Science Advances*, 3(2), February 2017. ISSN 2375-2548. DOI: [10.1126/sciadv.1601540](https://doi.org/10.1126/sciadv.1601540). URL <http://dx.doi.org/10.1126/sciadv.1601540>.
- [28] M. Akhtar, F. Bonus, F. R. Lebrun-Gallagher, N. I. Johnson, M. Siegele-Brown, S. Hong, S. J. Hile, S. A. Kulmiya, S. Weidt, and W. K. Hensinger. A high-fidelity quantum matter-link between ion-trap microchip modules. *Nature Communications*, 14(1), February 2023. ISSN 2041-1723. DOI: [10.1038/s41467-022-35285-3](https://doi.org/10.1038/s41467-022-35285-3). URL <http://dx.doi.org/10.1038/s41467-022-35285-3>.
- [29] Madelyn Cain, Chen Zhao, Hengyun Zhou, Nadine Meister, J. Pablo Bonilla Ataides, Arthur Jaffe, Dolev Bluvstein, and Mikhail D. Lukin. Correlated decoding of logical algorithms with transversal gates, 2024.
- [30] Kwok Ho Wan, Mark Webber, Austin G. Fowler, and Winfried K. Hensinger. An iterative transversal CNOT decoder, 2024. URL <https://arxiv.org/abs/2407.20976>.
- [31] Daniel Litinski. Magic state distillation: Not as costly as you think. *Quantum*, 3:205, December 2019. ISSN 2521-327X. DOI: [10.22331/q-2019-12-02-205](https://doi.org/10.22331/q-2019-12-02-205). URL <http://dx.doi.org/10.22331/q-2019-12-02-205>.
- [32] Universal Quantum team et. al. The impact of high-fidelity long-range connectivity on reaching quantum advantage in the fault tolerant regime. In preparation.
- [33] Universal Quantum team et. al. Transversal CNOT versus lattice surgery as a function of qubit connectivity costs. In preparation.
- [34] H. J. Briegel, D. E. Browne, W. Dür, R. Raussendorf, and M. Van den Nest. Measurement-based quantum computation. *Nature Physics*, 5(1):19–26, January 2009. ISSN 1745-2481. DOI: [10.1038/nphys1157](https://doi.org/10.1038/nphys1157). URL <http://dx.doi.org/10.1038/nphys1157>.
- [35] Riddhi S. Gupta, Neereja Sundaresan, Thomas Alexander, Christopher J. Wood, Seth T. Merkel, Michael B. Healy, Marius Hillenbrand, Tomas Jochym-O’Connor, James R. Wootton, Theodore J. Yoder, Andrew W. Cross, Maika Takita, and Benjamin J. Brown. Encoding a magic state with beyond break-even fidelity. *Nature*, 625(7994):259–263, January 2024. ISSN 1476-4687. DOI: [10.1038/s41586-023-06846-3](https://doi.org/10.1038/s41586-023-06846-3). URL <http://dx.doi.org/10.1038/s41586-023-06846-3>.
- [36] $[[7, 1, 3]]$ Steane code. In Victor V. Albert and Philippe Faist, editors, *The Error Correction Zoo*. 2024. URL <https://errorcorrectionzoo.org/c/steane>.
- [37] $[[15, 1, 3]]$ quantum Reed-Muller code. In Victor V. Albert and Philippe Faist, editors, *The Error Correction Zoo*. 2024. URL https://errorcorrectionzoo.org/c/stab_15_1_3.

- [38] Michael E. Beverland, Aleksander Kubica, and Krysta M. Svore. Cost of universality: A comparative study of the overhead of state distillation and code switching with color codes. *PRX Quantum*, 2: 020341, Jun 2021. DOI: [10.1103/PRXQuantum.2.020341](https://doi.org/10.1103/PRXQuantum.2.020341). URL <https://link.aps.org/doi/10.1103/PRXQuantum.2.020341>.
- [39] Craig Gidney, Michael Newman, and Matt McEwen. Benchmarking the planar honeycomb code. *Quantum*, 6:813, September 2022. ISSN 2521-327X. DOI: [10.22331/q-2022-09-21-813](https://doi.org/10.22331/q-2022-09-21-813). URL <http://dx.doi.org/10.22331/q-2022-09-21-813>.
- [40] Victor V. Albert and Philippe Faist, editors. *The Error Correction Zoo*. 2024. URL <https://errorcorrectionzoo.org/>.
- [41] Craig Gidney. Cleaner magic states with hook injection, 2023. URL <https://arxiv.org/abs/2302.12292>.
- [42] Craig Gidney. Stim: a fast stabilizer circuit simulator. *Quantum*, 5:497, July 2021. ISSN 2521-327X. DOI: [10.22331/q-2021-07-06-497](https://doi.org/10.22331/q-2021-07-06-497). URL <https://doi.org/10.22331/q-2021-07-06-497>.
- [43] Oscar Higgott and Craig Gidney. Py-matching v2. <https://github.com/oscarhiggott/PyMatching>, 2022.
- [44] Matt McEwen, Dave Bacon, and Craig Gidney. Relaxing hardware requirements for surface code circuits using time-dynamics. *Quantum*, 7:1172, November 2023. ISSN 2521-327X. DOI: [10.22331/q-2023-11-07-1172](https://doi.org/10.22331/q-2023-11-07-1172). URL <http://dx.doi.org/10.22331/q-2023-11-07-1172>.
- [45] Hector Bombin, Daniel Litinski, Naomi Nickerson, Fernando Pastawski, and Sam Roberts. Unifying flavors of fault tolerance with the ZX calculus. *Quantum*, 8:1379, June 2024. ISSN 2521-327X. DOI: [10.22331/q-2024-06-18-1379](https://doi.org/10.22331/q-2024-06-18-1379). URL <http://dx.doi.org/10.22331/q-2024-06-18-1379>.
- [46] Aleks Kissinger and John van de Wetering. Simulating quantum circuits with ZX-calculus reduced stabiliser decompositions. *Quantum Science and Technology*, 7(4):044001, July 2022. ISSN 2058-9565. DOI: [10.1088/2058-9565/ac5d20](https://doi.org/10.1088/2058-9565/ac5d20). URL <http://dx.doi.org/10.1088/2058-9565/ac5d20>.
- [47] Alexander M. Dalzell, Sam McArdle, Mario Berta, Przemyslaw Bienias, Chi-Fang Chen, András Gilyén, Connor T. Hann, Michael J. Kastoryano, Emil T. Khabiboulline, Aleksander Kubica, Grant Salton, Samson Wang, and Fernando G. S. L. Brandão. Quantum algorithms: A survey of applications and end-to-end complexities, 2023. URL <https://arxiv.org/abs/2310.03011>.
- [48] Creating a labeled tetrahedron with tikzpicture. <https://tex.stackexchange.com/questions/174317>. Accessed: 2024-10-21.